[AMERICAN JOURNAL OF SCIENCE, VOL. 260, OCTOBER 1962, P. 611-634]

THE JOIN $Ca_3Al_2Si_3O_{12}$–$Mg_3Al_2Si_3O_{12}$ AND ITS BEARING ON THE SYSTEM CaO–MgO–Al_2O_3–SiO_2 AT ATMOSPHERIC PRESSURE

G. A. CHINNER* and J. F. SCHAIRER

Geophysical Laboratory, Carnegie Institution of Washington, Washington, D. C.

ABSTRACT. At atmospheric pressure the "garnet" join $Ca_3Al_2Si_3O_{12}$ (grossularite composition)–$Mg_3Al_2Si_3O_{12}$ (pyrope composition) is quaternary. Data on quenching runs for eleven compositions along the join are presented in table 2 and figure 2 and give the temperatures of two quaternary invariant points within the system CaO–MgO–Al_2O_3–SiO_2, viz., anorthite-wollastonite–pseudowollastonite–melilite–liquid (1205 ± 5°C), and anorthite–forsterite–spinel–cordierite–liquid (1280 ± 5°C).

The garnet join cuts three subsolidus tetrahedra, viz., anorthite–wollastonite–gehlenite–akermanite; anorthite–forsterite–gehlenite–akermanite; and anorthite–forsterite–spinel–cordierite. Subsolidus tetrahedra in the vicinity of the "garnet" join are: anorthite–akermanite–diopside–$CaSiO_3$; anorthite–akermanite–diopside–forsterite; anorthite–forsterite–spinel–gehlenite; anorthite–forsterite–diopside–enstatite; anorthite–forsterite–enstatite–cordierite; and anorthite–enstatite–cordierite–SiO_2. The liquidus relations on the bounding planes of most of the subsolidus tetrahedra are known from the data of previous workers, and from these, figure 4, showing the relationship between univariant lines and invariant points where liquid is present in the silica-rich portion of the system CaO–MgO–Al_2O_3–SiO_2, has been constructed.

From the viewpoint of igneous petrology, the line efgh of figure 4 represents the temperature maximum on the divariant surfaces that separates liquids taking a saturated (silica-rich) trend from those taking an undersaturated (melilite-rich) trend. It is shown that part of the line efgh runs within the tetrahedron anorthite–forsterite–diopside–enstatite, so that "simplified basalt" compositions within the system CaO–MgO–Al_2O_3–SiO_2 may take either the saturated or the undersaturated trend, depending on the relative amounts of "normative" olivine, anorthite, diopside, and hypersthene. The classic gabbro-norite sequence produced by the contamination of basic rock with argillaceous material is illustrated in terms of the synthetic system, and it is suggested that the garnet- and cordierite-bearing magmatic rocks found at igneous contacts, rather than representing the end product of the gabbro-norite contamination sequence, may sometimes have been formed by the fractional melting of country rock.

INTRODUCTION

Recent high-pressure studies of phase equilibrium in the garnet family carried out at the Geophysical Laboratory have included determinations along the join grossularite ($Ca_3Al_2Si_3O_{12}$)–pyrope ($Mg_3Al_2Si_3O_{12}$) at 29 kilobars (Chinner, Boyd, and England, 1960) and at 10 kilobars water pressure (Yoder and Chinner, 1960). The stabilities of garnet solid solutions along this join are strongly dependent on the pressures of formation. At 29 kilobars and 1250°C, a complete series of solid solutions may be formed, but at 10 kilobars water pressure and 950°C, only garnets within the narrow range $Gro_{100}Py_0$–$Gro_{94}Py_6$ are stable. At atmospheric pressure neither grossularite nor pyrope is stable above approximately 850°, the temperature below which a glass will not crystallize in a reasonable length of time. However, the join lies in a strategic position within the quaternary system CaO–MgO–Al_2O_3–SiO_2, and we therefore considered it worthwhile to determine the liquidus and solidus relations along it. The results give information both for the understanding of relations within the system CaO–MgO–Al_2O_3–SiO_2 and for the interpretation of the more complex assemblages found in the hydrothermal study.

* Now at Department of Mineralogy and Petrology, University of Cambridge, England.

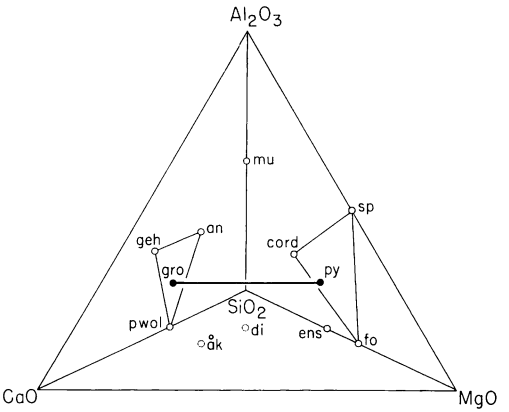

Fig. 1. The position of the join grossularite–pyrope and phases present in the silica-rich portion of the system CaO–MgO–Al_2O_3–SiO_2. Abbreviations for phases in this, and in succeeding diagrams: gro, grossularite; py, pyrope; pyrox, pyroxene; ens, enstatite; di, diopside; fo, forsterite; sp, spinel; sap, sapphirine; cord, cordierite; mu, mullite; mel, melilite; geh, gehlenite; ak, akermanite; an, anorthite; pwol, pseudowollastonite; wol, wollastonite; co, corundum; tr, tridymite; cr, cristobalite.

EXPERIMENTAL PROCEDURE

The Geophysical Laboratory quenching technique (Schairer, 1959) was used in all of the runs, the phases present being identified by optical examination and by X-ray diffractometer patterns. The determination of the temperature of beginning of melting for each composition studied requires some comment. Powdered charges of totally crystallized glasses were held at the appropriate temperatures; if the charge remained as a loose powder, liquid was assumed to be absent, whereas the fritting of the charge was taken as evidence of the presence of liquid. This method proved most unsatisfactory. In some of the compositions studied the amount of liquid present at the invariant points or univariant lines is very small, and in the earlier work insufficient time was allowed for equilibrium to be attained. Thus "beginning of melting" temperatures that appear to have been over 50° too high were obtained; these led to erroneous interpretations in a preliminary diagram previously published

TABLE 1

Initial treatment for crystallizing glasses used in quenching experiments

Composition	R. I. of glass	T, °C	Time, days
grossularite	1.614	1180	6
$Gro_{95}Py_5$	1.612	1160	7
$Gro_{90}Py_{10}$	1.610	1160	7
$Gro_{85}Py_{15}$	1.608	1160	14
$Gro_{80}Py_{20}$	1.607	1160	7
$Gro_{70}Py_{30}$	1.603	1050	14
$Gro_{60}Py_{40}$	1.600	1050	14
$Gro_{50}Py_{50}$	1.597	1050	14
$Gro_{40}Py_{60}$	1.595	1050	14
$Gro_{30}Py_{70}$	1.592	1230	7
$Gro_{20}Py_{80}$	1.591	1230	7
$Gro_{10}Py_{90}$	1.589	1230	7
Pyrope	1.587	1215	7

(Chinner and Schairer, 1959). The time and temperatures of crystallization of charges finally used are shown in table 1.

The composition of melilites in the various mixtures were determined from X-ray diffractometer patterns, using the method of Ervin and Osborn (1949). Due to the interference of peaks of the other minerals present, only the very intense (211) peak, with $Si_{(111)}$ as standard, could be used. This method gave consistent results for a series of test melilites prepared at 10 weight percent intervals along the join gehlenite–akermanite. However, the small difference between $d_{(211)}$ of gehlenite (2.846 Å) and $d_{(211)}$ of akermanite (2.873 Å) indicates that the precision of the melilite compositions quoted is no better than ± 5 molecular percent of either end member.

The Grossularite Composition

Within the subsolidus region the grossularite composition, lying in the system CaO–Al_2O_3–SiO_2, is represented by the assemblage anorthite–gehlenite–pseudowollastonite, or, below 1125° and above 850°, anorthite–gehlenite–wollastonite. The behavior of glasses of this composition has previously been discussed in detail by Yoder (1950); our data (table 2) agree with those of Yoder within the limits of error.

The Pyrope Composition

The pyrope composition lies within the system MgO–Al_2O_3–SiO_2, studied by Rankin and Merwin (1918); our data (table 2) agree substantially with theirs.

A point of interest for the pyrope composition lies in the disposition of the alternative tie lines forsterite–cordierite and enstatite–spinel. The original work of Rankin and Merwin indicated that forsterite–cordierite is the stable tie line at immediately subsolidus temperatures, the pyrope composition being represented by the assemblage forsterite–cordierite–spinel. In view of the widespread occurrence of enstatite–spinel in natural rocks of high Mg/Fe ratio, Tilley (1923) suggested that enstatite–spinel is a low temperature join and forsterite–cordierite is the high-temperature one.

Yoder (1952), working in the system MgO–Al_2O_3–SiO_2–H_2O at 1000 bars pressure, found no evidence of a join enstatite–spinel; Roy and Roy (1955), working in the same system at 10,000 psi pressure, obtained enstatite–cordierite–spinel assemblages, but, as the join forsterite–cordierite appeared to be stable at both higher and lower pressures within equivalent temperature ranges, they concluded that the enstatite was metastable. More recently, Yoder and Chinner (1960) have shown that at 10,000 bars water pressure the join forsterite–cordierite is cut by two joins, enstatite–sapphirine and enstatite–spinel, suggesting that the latter are really high-pressure joins.

Experiments were conducted on the pyrope composition to see whether the join enstatite–spinel is not also a low-temperature join. At subsolidus temperatures above 1140°, glasses of pyrope composition crystallize completely to the stable assemblage forsterite–cordierite–spinel, which begins to melt at the ternary invariant point forsterite–cordierite–spinel–liquid, at 1370 ± 5°C. Below 1140°, such glasses crystallize to a mixture of orthoenstatite, cordierite,

TABLE 2

Results of quenching experiments

Abbreviations as in figure 1; gl = glass
( ) = identification uncertain. ? = unidentified phase.

T°C	Time, hrs	Results
	Grossularite composition	
1346	5	gl
1341	5	geh, gl
1290	24	geh, gl
1285	24	an, geh, gl
1270	48	glazed charge; an, geh, pwol
1265	48	unfritted charge, an, geh, pwol
	$Gro_{95}Py_5$ composition	
1210	48	fritted, pwol, an, mel
1197	72	fritted, pwol, wol, an, mel
1190	72	unfritted, pwol, wol, an, mel
1185	48	unfritted, pwol, wol, an, mel
1175	144	unfritted, wol, an, mel
	$Gro_{90}Py_{10}$ composition	
1305	42	gl
1300	24	mel, an, gl
1255	41	mel, an, gl
1250	48	pwol, mel, an, gl
1210	48	fritted; pwol, mel, an
1197	72	fritted; wol, mel, an
1185	48	fritted; wol, mel, an
1175	144	unfritted; wol, mel, an
	$Gro_{85}Py_{15}$ composition	
1175	144	fritted; mel, an, (wol)
1170	96	unfritted; mel, an, (wol)
	$Gro_{80}Py_{20}$ composition	
1320	5	gl
1315	24	an, gl
1285	48	an, gl
1280	24	mel, an, gl
1255	72	mel, an, gl
1200	168	fritted; mel, an, ?
1175	144	fritted; mel, an, ?
1170	96	fritted; mel, an, ?
	$Gro_{70}Py_{30}$ composition	
1340	24	gl
1335	24	sp, gl
1330	24	sp, gl
1325	24	an, sp, gl
1265	72	an, sp, gl
1260	72	mel, an, sp, gl
1240	96	mel, an, sp, gl
1235	48	mel, an, pyrox, gl
1230	48	mel, an, pyrox, gl
1225	96	mel, an, pyrox, gl
1220	96	mel, an, pyrox, gl
1215	96	mel, an, gl, ?
1210	72	mel, an, gl, ?
1200	168	mel, an, gl, ?
1180	144	fritted, mel, an, (fo)
1175	96	fritted, mel, an, (fo)
1170	96	unfritted, mel, an, (fo)

TABLE 2 (Continued)

T°C	Time, hrs	Results
	$Gro_{60}Py_{40}$ composition	
1390	6	sp, gl
1330	24	sp, gl
1325	72	an, sp, gl
1275	96	an, sp, gl
1270	72	fo, an, sp, gl
1240	96	fo, an, sp, gl
1235	48	mel, an, pyrox, (fo), gl
1230	48	mel, an, pyrox, (fo), gl
1225	96	mel, an, gl, ?
1220	96	mel, an, pyrox, (fo), gl
1215	96	mel, an, pyrox, (fo), gl
1210	72	mel, an, fo, gl
1200	168	fritted, mel, an, fo
1175	96	fritted, mel, an, fo
1170	96	unfritted, mel, an, fo
	$Gro_{50}Py_{50}$ composition	
1440	2	gl
1435	48	sp, gl
1320	5	sp, gl
1315	24	an, sp, gl
1310	24	an, sp, gl
1305	42	fo, an, sp, gl
1245	96	fo, an, sp, gl
1240	72	fo, an, sp, gl
1235	72	fo, an, mel, pyrox, (sp), gl
1230	48	fo, an, mel, pyrox, (sp), gl
1225	24	fo, an, mel, gl
1220	96	fo, an, mel, gl
1215	96	fo, an, mel, gl
1210	72	fo, an, mel, gl
1200	168	fo, an, mel, gl
1180	144	fritted; fo, an, mel
1175	96	fritted; fo, an, mel
1170	96	fritted; fo, an, mel
	$Gro_{40}Py_{60}$ composition	
1475	4	gl
1470	3	sp, gl
1355	24	sp, gl
1350	19	fo, sp, gl
1320	24	fo, sp, gl
1315	24	an, fo, sp, gl
1240	72	an, fo, mel, gl
1235	72	an, fo, mel, gl
1230	24	an, fo, (mel), gl
1225	72	an, fo, (mel), gl
1215	96	an, fo, (mel), gl
1175	96	fritted; an, fo, (mel)
1170	96	unfritted; an, fo, (mel)
	$Gro_{30}Py_{70}$ composition	
1500	1	gl
1495	1½	sp, gl
1395	24	sp, gl
1390	18	fo, sp, gl
1315	48	fo, sp, gl
1310	72	an, fo, sp, gl
1280	96	an, fo, sp, gl
1275	96	unfritted; cord, an, fo, sp

TABLE 2 (Continued)

T°C	Time, hrs	Results
	$Gro_{20}Py_{80}$ composition	
1520	2	gl
1510	1½	sp, gl
1505	1½	sp, gl
1420	18	sp, gl
1415	20	fo, sp, gl
1300	24	an, fo, sp, gl
1295	44	an, fo, sp, gl
1285	72	an, fo, sp, gl
1280	96	fritted; cord, an, fo, sp
1275	96	unfritted; cord, an, fo, sp
	$Gro_{10}Py_{90}$ composition	
1525	1½	gl
1520	2	sp, gl
1445	24	sp, gl
1440	24	fo, sp, gl
1330	48	fo, sp, gl
1325	72	cord, fo, sp, gl
1285	72	cord, fo, sp, gl
1280	96	fritted; an, cord, fo, sp
1275	96	unfritted; an, cord, fo, sp
	Pyrope composition	
1530	1½	gl
1525	1½	sp, gl
1458	24	sp, gl
1453	21	fo, sp, gl
1375	22	fo, sp, gl
1370	24	fo, sp, gl
1365	24	fritted; cord, fo, sp
1360	68	unfritted; cord, fo, sp

spinel, and small amounts of forsterite. Such a mixture will lose all, or nearly all of its orthoenstatite when heated for several days above 1140°. Below 1140°, however, reaction rates are apparently too low for equilibrium to be attained in any reasonable time. Heating these mixtures at 1130° for periods of up to four months produced no recognizable growth of forsterite and cordierite at the expense of enstatite and spinel, or vice-versa: it is therefore impossible by this method to tell which of these alternative tie lines is stable below 1140°C. However, in preliminary experiments on the pyrope composition at 2000 bars H_2O pressure and 850°C it was found that a glass would crystallize initially to an aggregate of orthoenstatite, forsterite, cordierite, and spinel, the enstatite gradually disappearing after periods of six to ten days to give only forsterite, cordierite, and spinel. In this case the enstatite is clearly metastable. We therefore consider that in the dry system the join enstatite–spinel is also metastable, the appearance of orthoenstatite being due to an ease of nucleation greater than that of the stable phases. The fact that enstatite does not form in the pyrope composition above 1140° may well be due to the existence above this temperature of the possibly less readily nucleated protoenstatite as the stable $MgSiO_3$ polymorph, as well as to increased reaction rates. Resolution of this question must presumably await more complete knowledge of the polymorphic transitions in the pyroxene group.

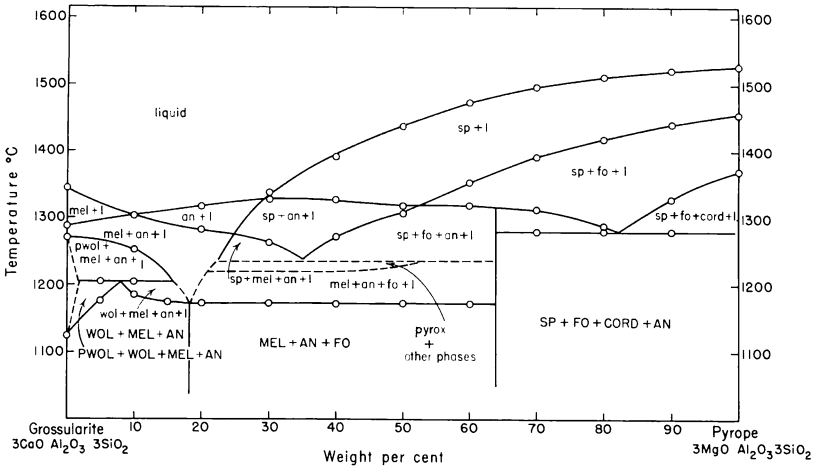

Fig. 2. Temperature/composition plot of the results on the join grossularite–pyrope presented in table 2. Abbreviations as in figure 1: l = liquid.

The Join "Grossularite"–"Pyrope"

Although no experiments have previously been made on the garnet compositions, many of the neighboring ternary planes and binary joins have been studied. These data will subsequently be combined to give a picture of the subsolidus phase volumes, quaternary invariant points, and univariant lines in this portion of the system CaO–MgO–Al_2O_3–SiO_2.

Data on the "garnet" join are tabulated in table 2, and are graphically presented on the temperature-composition projection of figure 2. The essential features of this diagram are the result of the specialized position of the "garnet" join in the system CaO–MgO–Al_2O_3–SiO_2.

By the equation

grossularite + pyrope → anorthite + forsterite.

$$Ca_3Al_2Si_3O_{12} + 2Mg_3Al_2Si_3O_{12} = 3CaAl_2Si_2O_8 + 3Mg_2SiO_4$$

the garnet join intersects the line anorthite–forsterite at a composition of $Gro_{36}Py_{64}$ (weight percent). Similarly, by the equation

grossularite + pyrope → anorthite + gehlenite + akermanite

$$4Ca_3Al_2Si_3O_{12} + Mg_3Al_2Si_3O_{12} = 4CaAl_2Si_2O_8 + Ca_2Al_2SiO_7 + 3Ca_2MgSi_2O_7$$

a composition $Gro_{82}Py_{18}$ can be represented by a mixture of anorthite and a melilite of composition $Geh_{25}Ak_{75}$. Within the median range $Gro_{82}Py_{18}$ to $Gro_{36}Py_{64}$, the garnet compositions can therefore be represented in the subsolidus by varying proportions of anorthite, forsterite, and a melilite $Geh_{25}Ak_{75}$. The compositions of melilites in garnet mixtures within this range have been determined by the X-ray method and agree with the calculated value (fig. 3) to within the limits of error.

Below the temperatures of the wollastonite-pseudowollastonite inversion, garnet compositions within the range Gro_{100} to $Gro_{82}Py_{18}$ are represented in the subsolidus by varying proportions of anorthite, wollastonite, and melilite, the melilite changing from pure gehlenite to $Geh_{25}Ak_{75}$. Figure 3 shows excel-

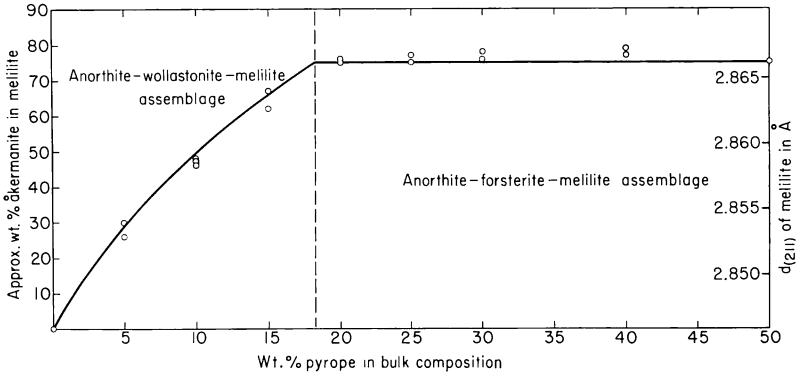

Fig. 3. Compositions of melilites in glasses crystallized at 1140° plotted against the bulk composition on the join grossularite–pyrope. Solid line denotes calculated melilite composition; circles denote compositions actually determined by measurement of $d_{(211)}$ of the melilites. Bulk compositions between $Gro_{50}Py_{50}$ and $Gro_{36}Py_{64}$ contain too little melilite for the melilite composition to be determined. Dashed line indicates theoretical intersection of the join grossularite–pyrope with the join anorthite–$Geh_{25}Ak_{75}$.

lent correspondence between the measured and calculated compositions of the melilites that form within this range.

Garnet compositions between $Gro_{36}Py_{64}$ and pyrope are represented by the subsolidus assemblage anorthite–forsterite–cordierite–spinel.

Univariant lines and invariant points.—The univariant paths involved in the crystallization of any garnet composition may be followed by reading vertically on the temperature-composition projection of figure 2. The letters (F, D, etc.) denoting the invariant points in the text are those used in the diagrammatic representation of the univariant lines and invariant points of figure 4, the derivation of which will be treated subsequently.

The assemblage spinel–forsterite–cordierite–anorthite begins to melt at 1280° ± 5°C, the temperature of the quaternary invariant point F, an–fo–cord–sp–liq. Garnet compositions descend to this point along the univariant lines cord–fo–sp–liq and an–fo–sp–liq.

Because garnet compositions between $Gro_{82}Py_{18}$ and $Gro_{36}Py_{64}$ are all represented in the subsolidus by varying proportions of anorthite, forsterite, and a melilite $Geh_{25}Ak_{75}$, they all begin to melt at the same temperature (1175° ± 5°C) along the univariant line an–fo–mel–liq. On cooling, these compositions descend towards the univariant line an–fo–mel–liq along the univariant lines an–fo–sp–liq and an–mel–sp–liq. At approximately 1235°, spinel disappears. The more magnesian compositions between approximately $Gro_{45}Py_{55}$ and $Gro_{36}Py_{64}$ apparently pass through the quaternary reaction point D, an–fo–sp–mel–liq, where spinel is lost and melilite gained, crystallization then proceeding with falling temperature along the univariant line an–fo–mel–liq. The more calcium-rich compositions between $Gro_{82}Py_{18}$ and $Gro_{70}Py_{30}$ do not pass through point D. A diopsidic pyroxene (identified by the $(22\bar{1})$ X-ray reflection at 30° 2θ, CuKα rad.) enters these compositions at approximately 1230° and disappears at approximately 1215°. Runs within this temperature and composition range yielded pyroxene associated variously with anorthite,

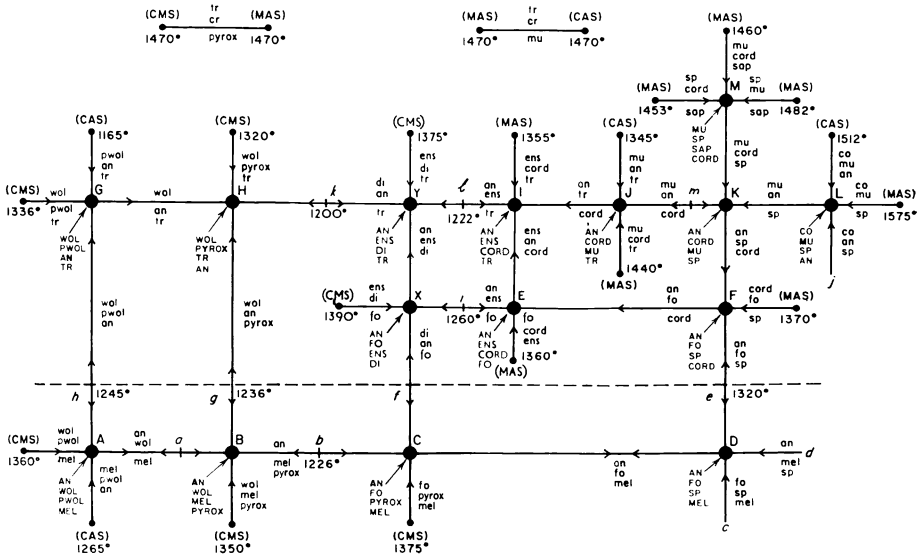

Fig. 4. The relation of ternary invariant points (small solid circles) in the limiting systems to univariant lines and quaternary invariant points (large solid circles, lettered in capitals) within the silica-rich portion of the system CaO–MgO–Al_2O_3–SiO_2. This diagram merely depicts phase relationships. The lines and points do not lie on a plane; their spatial angular relationships as shown, the length of lines, and the position of temperature maxima on these lines are arbitrary and without significance. Arrows indicate direction of falling temperature. Abbreviations for solid phases as in figure 1. References for temperatures given in tables 3 and 4.

melilite, forsterite, and glass, but as the pyroxene and forsterite content is so small, and the temperature range so narrow, it was not possible to determine the precise phase relationships involved. The pyroxene-containing area of figure 2 is thus purely diagrammatic. However, the appearance of pyroxene is doubtless related to the disappearance, by reaction, of spinel. As a more precisely determined example of the spinel-diopside relationship, one may use the join diopside–forsterite–anorthite, which lies close to the grossularite–pyrope join in the system CaO–MgO–Al_2O_3–SiO_2 (Osborn and Tait, 1952). Certain compositions close to the anorthite–forsterite join (Osborn and Tait, 1952, fig. 5) develop spinel at liquidus temperatures, and hence leave the plane diopside–forsterite–anorthite, eventually joining the univariant line an–fo–sp–liq via either of the divariant surfaces an–sp–liq or fo–sp–liq. Along the line an–fo–sp–liq, spinel dissolves as the temperature decreases. At 1317° the last of the spinel disappears, and the system gains one degree of freedom. The liquid thus leaves the univariant line and proceeds, with falling temperature, across the divariant plane an–fo–liq until 1270°, where the univariant line an–fo–pyrox–liq is reached, along which pyroxene crystallizes and liquid disappears.

In the case of the garnet join, compositions that later develop pyroxene (fig. 2) descend along the univariant lines an–fo–sp–liq and an–mel–sp–liq. Consideration of a solid model of the system CaO–MgO–Al_2O_3–SiO_2 shows that as the composition of a liquid on either of these univariant lines changes in

TABLE 3

Temperatures of univariant maxima and invariant points of figure 4

Abbreviations of phases given in legend of figures 1 and 4

Univariant maxima

a	an–wol–mel–liq	unknown
b	an–mel–pyrox–liq	1226°C (de Wys and Foster, 1958)
c	to high-MgO portion of system CaO–MgO–Al_2O_3–SiO_2.	
d	to high-Al_2O_3 portion of system. Connection between (d) and (j) given by DeVries and Osborn (1957), fig. 9.	
e	an–fo–sp–liq	1320°C (DeVries and Osborn, 1957)
f	di–an–fo–liq	unknown, but close to 1270°C (Osborn and Tait, 1952)
g	wol–an–pyrox–liq	1236°C (Osborn, 1942)
h	wol–pwol–an–liq	1245°C (Osborn, 1942)
i	an–ens–fo–liq	1260°C (Andersen, 1915)
j	see (d)	
k	di–an–tr–liq	~1200°C (Greig, unpublished data, see Osborn and Tait, 1952)
l	an–ens–tr–liq	1222°C (Andersen, 1915)
m	mu–an–cord–liq	unknown

Determined invariant points

A	An–wol–pwol–mel–liq	1205 ± 5°C
F	An–fo–sp–cord–liq	1280 ± 5°C

TABLE 4

Temperatures of ternary invariant points on figure 4

(MAS = MgO–Al_2O_3–SiO_2; CAS = CaO–Al_2O_3–SiO_2; CMS = CaO–MgO–SiO_2)

Abbreviations of phases given in legend of figure 1

Invariant point	Ternary system	T °C	Reference
mu–cord–sap–liq	MAS	1460±5	Keith and Schairer (1952)
sp–cord–sap–liq	MAS	1453±5	" " " "
sp–mu–sap–liq	MAS	1482±3	" " " "
pwol–an–tr–liq	CAS	1165±5	Schairer (1942, fig. 2)
wol–pyrox–tr–liq	CMS	1320±5	Ricker and Osborn (1954)
ens–di–tr–liq	CMS	~1375	Osborn and Muan (1960)
ens–cord–tr–liq	MAS	1355±5	Schreyer and Schairer (unpub.)
mu–an–tr–liq	CAS	1345±5	Schairer (1942, fig. 2)
co–mu–an–liq	CAS	1512±5	" " "
co–mu–sp–liq	MAS	1575±5	Rankin and Merwin (1918)
mu–cord–tr–liq	MAS	1440±5	Schreyer and Schairer (unpub.)
ens–di–fo–liq	CMS	~1390	Osborn and Muan (1960)
wol–pwol–tr–liq	CMS	1336±5	Ricker and Osborn (1954)
cord–fo–ens–liq	MAS	1364±5	Schairer (unpublished)
cord–fo–sp–liq	MAS	1370±5	Rankin and Merwin (1918)
wol–pwol–mel–liq	CMS	1360±5	Ricker and Osborn (1954)
mel–pwol–an–liq	CAS	1265±5	Schairer (1942, fig. 2)
wol–mel–di–liq	CMS	1350±5	Ricker and Osborn (1954)
fo–di–mel–liq	CMS	1357±5	" " " "
tr–cr–pyrox–liq	CMS	1470±10	" " " "
tr–cr–pyrox–liq	MAS	1470±10	Rankin and Merwin (1918)
tr–cr–mu–liq	MAS	1470±10	" " " "
tr–cr–mu–liq	CAS	1470±10	Schairer (1942, fig. 2)

response to temperature decrease spinel must dissolve (Osborn and Tait, 1952, p. 429). Disappearance of spinel before the invariant point D (fig. 4) is reached will cause the liquids to leave the lines an–fo–sp–liq and an–mel–sp–liq and to move across the divariant surfaces, an–fo–liq and an–mel–liq, respectively, to the univariant lines an–fo–pyrox–liq and an–mel–pyrox–liq. Loss of pyroxene in the garnet compositions at 1215° may occur at the invariant reaction point C, an–fo–pyrox–mel (fig. 4), although it seems possible that loss of pyroxene before C is reached could cause the system to again become divariant and to "bypass" the invariant point via the surfaces an–mel–liq and an–fo–liq to the univariant line an–fo–mel–liq, along which the liquids finally crystallize. Precise elucidation of these relationships must await investigation of more favorable compositions within the system CaO–MgO–Al_2O_3–SiO_2.

Below the temperature of the wollastonite-pseudowollastonite inversion, garnet compositions within the range Gro_{100} to $Gro_{82}Py_{18}$ are represented by the subsolidus assemblage wollastonite–melilite–anorthite. The more pyrope-rich of these compositions melt at intervals along the univariant line an–wol–mel–liq. and at 1205 ± 5°C pass through the invariant point A, an–wol–pwol–mel–liq. The more grossularite-rich compositions, however, undergo a subsolidus reaction of the type

$$wol_{s.s.} + an + mel_{s.s.} = wol + pwol_{s.s.} + an + mel_{s.s.},$$

and do not begin to melt until the temperature of the invariant point A (fig. 4) is reached. The phase rule requires that a small range of grossularite-rich compositions (with less than 5 percent pyrope) must be represented between 1125° and 1265° (fig. 2) by the three-phase assemblage $pwol_{s.s.}$–mel–an. Such compositions will begin to melt between 1205° and 1265°, along the univariant line pwol–mel–an–liq.

Subsolidus tetrahedra on the garnet join.—Since the garnet join cuts through several phase tetrahedra in the quaternary system, the crystallization paths given by our data are necessarily disconnected. The invariant points and univariant lines that connect these may, however, be deduced from a knowledge of the subsolidus phase tetrahedra and from the liquidus data of previous workers in the system. The subsolidus tetrahedra that represent the garnet compositions may be considered at a temperature below 1125°, where the variable pseudowollastonite-wollastonite inversion is no longer a complicating factor. The tetrahedra are most easily visualized with the aid of a solid model of the system CaO–MgO–Al_2O_3–SiO_2; however, as such a model is too complicated to represent in two dimensions, the tetrahedra are shown in "exploded" form in figure 5, and their relative positions may be seen by comparison with figure 1.

The garnet join cuts three tetrahedra:

(1) The tetrahedron anorthite–wollastonite–gehlenite–akermanite. Compositions within this tetrahedron are represented by three phases: wollastonite, anorthite, and a melilite solid solution.

(2) The tetrahedron anorthite–forsterite–gehlenite–akermanite. Compositions within this tetrahedron will normally be represented by anorthite, forsterite, and a melilite of varying composition. However, because the join

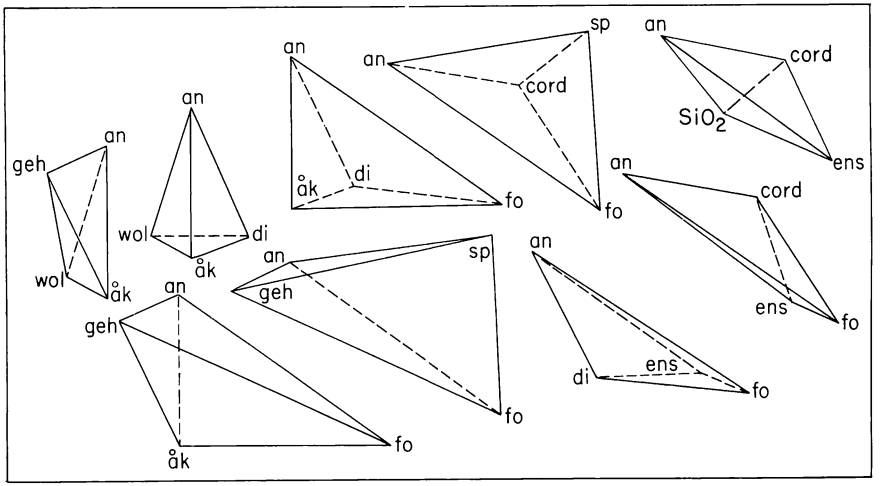

Fig. 5. Inferred subsolidus tetrahedra in the system CaO–MgO–Al_2O_3–SiO_2 at approximately 1125°C. Abbreviations as in figure 1.

grossularite–pyrope cuts the join anorthite–forsterite, the garnet join lies in a unique plane within the tetrahedron.

(3) The tetrahedron anorthite–forsterite–spinel–cordierite.

Neighboring subsolidus tetrahedra.—The tetrahedra in the vicinity of the garnet join involve the pyroxene solid solutions between diopside, enstatite, and alumina. Knowledge of the extent of these solid solutions is still very inadequate. Alumina substitutes in diopside by the scheme (Ca,Mg) Si → Al.Al; Segnit (1953) stated the maximum solid solution along the join diopside ($CaMgSi_2O_6$)–"Ca Tschermakite" ($CaAl_2SiO_6$) to be 25 weight percent $CaAl_2SiO_6$, and along the join diopside–"Mg Tschermakite" ($MgAl_2SiO_6$) to be 20 weight percent $MgAl_2SiO_6$. Other workers (Zvetkov, 1945; Sakata, 1957) consider that diopside can incorporate greater amounts of alumina than this, and place the limit of solid solution along the join diopside–"Ca Tschermakite" at between 30 and 40 weight percent $CaAl_2SiO_6$.

Earlier workers (Ricker and Osborn, 1954) considered that at subliquidus temperatures diopside and $MgSiO_3$ were completely miscible, but Boyd and Schairer (1957) show an immiscibility gap between 45 and 60 percent diopside at the solidus along the join $MgSiO_3$–diopside. In view of these uncertainties, in the following analysis the end members diopside and/or enstatite will be taken as the apices of pyroxene-bearing tetrahedra. The effect of solid solution involving these end members will be to remove temperature maxima and possibly to introduce minima into some of the univariant lines thus deduced; such possibilities will be discussed when the relevant lines are considered. In the following discussion the abbreviation "ens" will be used for the $MgSiO_3$-rich pyroxene, whether it be clinoenstatite, protoenstatite, or orthoenstatite.

The existence of the tetrahedron anorthite–forsterite–gehlenite–akermanite directly determines the configuration of the neighboring tetrahedra.

The presence of a plane forsterite–anorthite–akermanite would prohibit

any join between diopside and a melilite other than akermanite.[1] Two tetrahedra would thereby be generated:

anorthite–akermanite–gehlenite–forsterite,

anorthite–akermanite–diopside–forsterite.

Similarly, since the join gehlenite–forsterite cuts the join spinel–akermanite.

$$\underset{\text{forsterite}}{Mg_2SiO_4} + \underset{\text{gehlenite}}{Ca_2Al_2SiO_7} = \underset{\text{akermanite}}{Ca_2MgSi_2O_7} + \underset{\text{spinel}}{MgAl_2O_4}$$

The existence of a forsterite–gehlenite–anorthite plane would prohibit any join between spinel and a melilite other than gehlenite.[2]

The tetrahedron anorthite–forsterite–spinel–gehlenite would thus be generated.

For the tetrahedra involving enstatite, it is known (Andersen, 1915) that anorthite, forsterite, and clinoenstatite are compatible phases at the solidus; the plane containing these three minerals prohibits the join cordierite–diopside, so two tetrahedra are generated:

anorthite–forsterite–diopside–enstatite,

anorthite–forsterite–enstatite–cordierite.

The remaining tetrahedron of interest here is the silica-rich tetrahedron

anorthite–enstatite–cordierite–silica.

Crystallization paths in the silica-rich portion of the system CaO–MgO–Al_2O_3–SiO_2.—Given the subsolidus tetrahedra and liquidus data for the planes bounding them, it is possible to deduce the relationship of univariant lines and invariant points where liquid is present within the system CaO–MgO–Al_2O_3–SiO_2.

The simple geometrical principles involved are similar to those used in deducing maxima, minima, reaction points, and eutectics in a ternary system, and have been discussed in detail by Schairer (1942). In brief, these may be stated:

If a univariant line pierces two faces of a tetrahedron, the line passes through that tetrahedron without involvement in an invariant point within the tetrahedron.

If the piercing point of a univariant line is found on only one bounding face of a tetrahedron, that univariant line "ends" at a quaternary invariant point within the tetrahedron.

If the composition of a quaternary invariant point lies within the tetrahedron formed by its four solid phases, the invariant point is a eutectic.

If the composition of a quaternary invariant point lies outside the tetrahedron formed by the four solid phases in equilibrium with liquid at that point, it is a reaction point.

Liquidus data for many of the planes bounding the tetrahedra in this portion of the system have been determined previously: approximate liquidus

[1] There is no conclusive evidence for this, as the data from the grossularite–pyrope join indicate only that spinel is incompatible with any melilite richer in akermanite than Ak_{75}, and that diopside is incompatible with any melilite poorer in akermanite than Ak_{75}. However, the compatibility of spinel with akermanite-poor melilites other than gehlenite, and the compatibility of diopside with gehlenite-poor melilites other than akermanite, would not affect the general applicability of this discussion.

[2] See footnote 1.

relationships for those planes as yet undetermined may be derived from the 5, 10, 15, 20, 25, 30, and 35 percent Al_2O_3 planes studied by Osborn and others (1954), and from the 10 percent MgO plane studied by Prince (1954). For example, the unknown plane anorthite–akermanite–forsterite cuts all of the equal-alumina planes of Osborn and others (1954), as well as the 10 percent MgO plane. Each equal-alumina or equal-magnesia plane will thus have one line in common with the plane anorthite–akermanite–forsterite (light dashed lines in fig. 6). The points of intersection of three-phase boundaries with the common lines on the diagrams of Osborn and others, and Prince (1954) may be transferred to the plot of the appropriate common line on a diagram of the plane an–ak–fo; these points of intersection, when joined, give the three-phase boundaries on the unknown plane. In figure 6 the planes an–$CaSiO_3$–ak, an–geh–ak, an–geh–fo, an–ak–fo, fo–geh–ak, an–fo–cord, an–ens–cord, and an–SiO_2–cord, derived by this method, are shown.

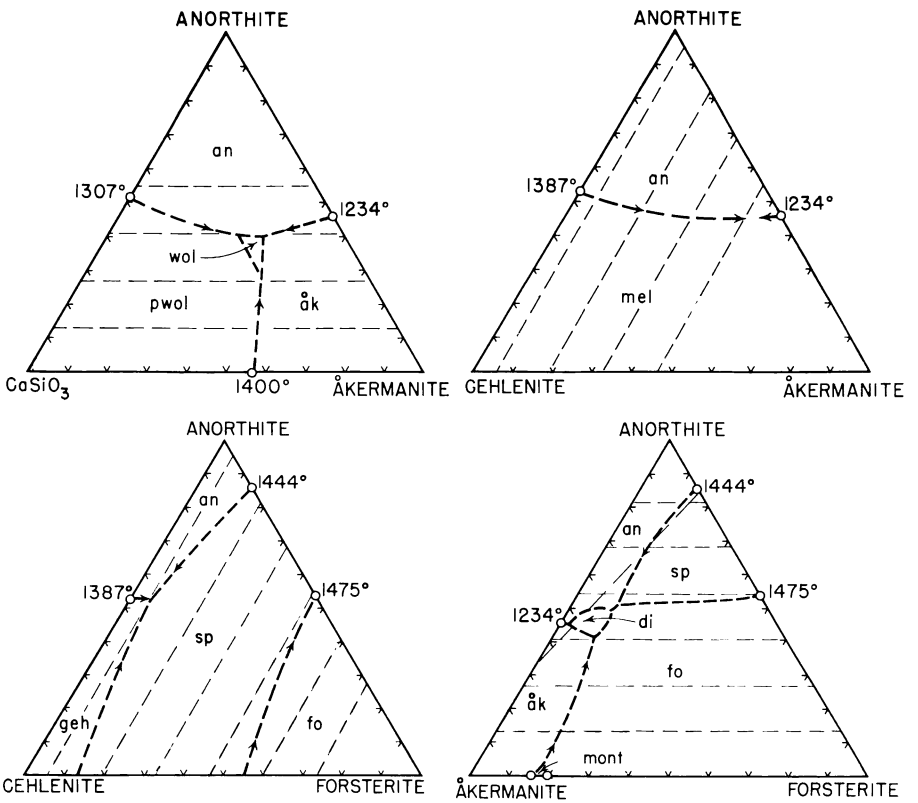

Fig.6. Configuration of liquidus surfaces and piercing points on planes within the system CaO–MgO–Al_2O_3–SiO_2, derived from the data of Osborn and others (1954) and Prince (1954). Abbreviations as in figure 1. Light dashed lines within each triangle indicate the lines of intersection of that plane with the planes of equal-alumina content studied by Osborn and others and with the 10 percent MgO plane studied by Prince which were used in the construction of the figures.

Figure 4 presents in the diagrammatic "flow sheet" form of Schairer (1942) the relationship between univariant lines and invariant points deduced from the liquidus data and the subsolidus tetrahedra. The deduction of this "flow sheet" is now briefly described in terms of the individual tetrahedra (fig. 5).

(1) The tetrahedron *anorthite–$CaSiO_3$–gehlenite–akermanite*. At temperatures above 1125° this includes the variable tetrahedron an–pwol–wol–mel, and. due to the changing composition of the wollastonite along the join $CaSiO_3$–diopside, this tetrahedron will "transgress" to a small extent the tetrahedron anorthite–akermanite–diopside–$CaSiO_3$. Of the faces bounding this tetrahedron:

(i) Pseudowollastonite–gehlenite–akermanite (Osborn and Schairer, 1942) has a minimum.

(ii) Anorthite–gehlenite–pseudowollastonite (Rankin and Wright, 1915) has a piercing point. mel–pwol–an–liq.

(iii) Anorthite–gehlenite–akermanite (fig. 6) has a minimum.

(iv) Anorthite–$CaSiO_3$–akermanite is shown in figure 6 as containing three piercing points wol–pwol–an–liq. wol–pwol–ak–liq, and an–wol–ak–liq.

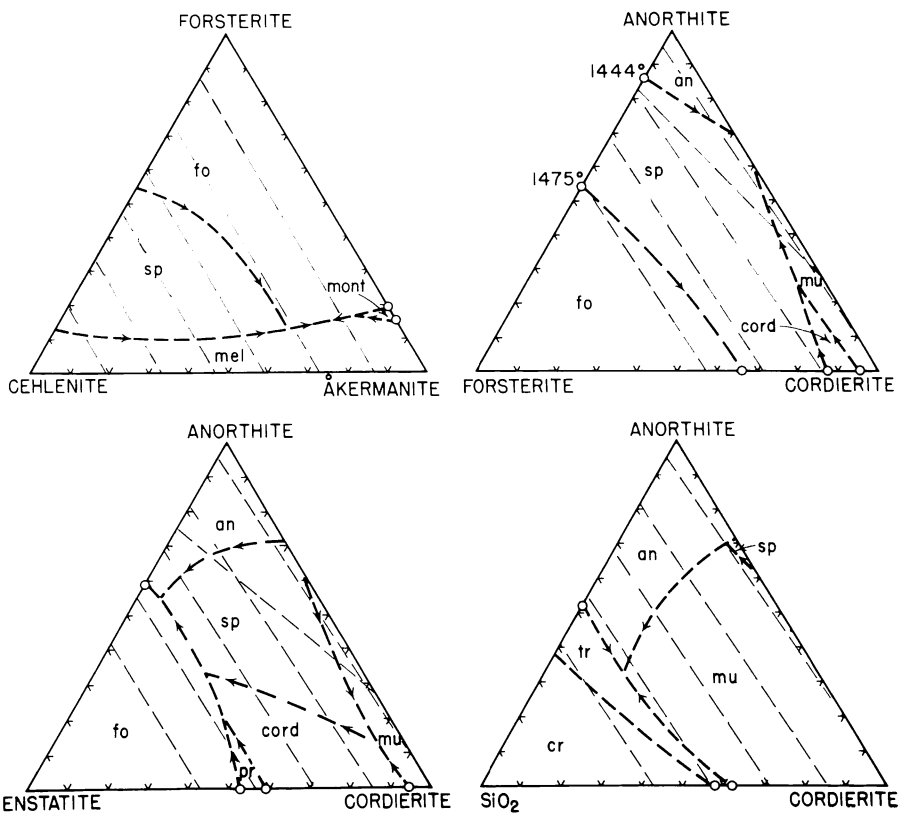

The small field of wollastonite on this plane is required by our own data, which suggest the existence of a univariant line an–wol–mel–liq. Osborn and others (1954) give no data to support this, but it is possible that the refinement of their work was insufficient to determine the tiny field of wollastonite which this interpretation suggests should be present on their 15 percent plane.

Within the tetrahedron an–$CaSiO_3$–geh–ak the three univariant lines mel–pwol–an–liq, wol–pwol–an–liq, and wol–pwol–mel–liq will meet at the quaternary reaction point A (fig. 4), an–wol–pwol–mel–liq, shown by our data to be at 1205° ± 5°. Proceeding from this reaction point with decreasing temperature is the univariant line an–wol–mel–liq, which has a temperature maximum where it intersects the plane an–wol–ak and a quaternary minimum between this maximum and the position of the quaternary reaction point A (fig. 4). Data on the join grossularite–pyrope indicate that the composition of the melilite at this minimum is more akermanite rich than $Geh_{25}Ak_{75}$ and that the temperature of the minimum is less than 1170°.

(2) The tetrahedron *$CaSiO_3$–anorthite–diopside–akermanite* shares with the preceding tetrahedron the plane anorthite–$CaSiO_3$–akermanite. Liquidus relations on the three other bounding planes are known:

(i) $CaSiO_3$–diopside–anorthite (Osborn, 1942) contains the piercing points wol–pwol–an–liq, and wol–an–pyrox–liq.

(ii) $CaSiO_3$–diopside–akermanite (Ricker and Osborn, 1954) contains the piercing points wol–pwol–ak–liq and wol–ak–di–liq.

(iii) Diopside–anorthite–akermanite (de Wys and Foster, 1958) contains a piercing point, di–an–ak–liq.

Within the tetrahedron, therefore, two univariant lines, wol–pwol–an–liq and wol–pwol–mel–liq, descend from temperature maxima on, respectively, the planes $CaSiO_3$–an–di and $CaSiO_3$–di–ak, and pass through the plane an–ak–$CaSiO_3$ on their way to the quaternary reaction point an–wol–pwol–mel–liq. A (fig. 4). The "ternary" eutectics on each of the four faces will form temperature maxima on four univariant lines, which will meet at the quaternary eutectic B, wol–an–di–ak–liq (fig. 4).

(3) The tetrahedron *anorthite–diopside—akermanite–forsterite* shares with the preceding tetrahedron the plane di–an–ak. Liquidus relations on the three other bounding faces have been determined:

(i) Diopside–forsterite–anorthite (Osborn and Tait, 1952) contains piercing points an–fo–sp–liq and di–an–fo–liq.

(ii) Anorthite–akermanite–forsterite (fig. 6) contains a piercing point, an–fo–sp–liq, and three piercing points involving pyroxene, an–mel–di–liq, di–an–fo–liq, and fo–di–mel–liq. The piercing point involving monticellite will be ignored, as no invariant points involving monticellite are found in the portion of the system under discussion;

(iii) Forsterite–akermanite–diopside (Ricker and Osborn, 1954) contains a piercing point, fo–di–ak–liq. The piercing point involving monticellite will be ignored.

The tetrahedron contains no invariant point. The four univariant lines, an–fo–sp–liq, pyrox–an–fo–liq, fo–pyrox–mel–liq, and an–mel–pyrox–liq, all move across the tetrahedron with decreasing temperature, and pass through the

plane anorthite–akermanite–forsterite into the adjoining tetrahedron anorthite–gehlenite–akermanite–forsterite. The piercing points on the planes an–fo–di. an–ak–di, and ak–di–fo will probably lie close to temperature maxima on the univariant lines, respectively, an–fo–pyrox–liq, an–mel–pyrox–liq, and mel–pyrox–fo–liq.

(4) The tetrahedron *anorthite–gehlenite–akermanite–forsterite.* The bounding planes are all shown in figure 6:

(i) Anorthite–gehlenite–akermanite, already discussed, contains a minimum, an–mel–liq.

(ii) Anorthite–gehlenite–forsterite contains a piercing point, an–geh–sp–liq.

(iii) Gehlenite–akermanite–forsterite appears to contain a piercing point, fo–mel–sp–liq. and a minimum, fo–mel–liq.

(iv) Anorthite–akermanite–forsterite, already discussed, contains four piercing points, an–fo–sp–liq, an–ak–di–liq, an–pyrox–fo–liq, ak–pyrox–fo–liq.

The tetrahedron thus contains two invariant points: an–fo–sp–mel–liq (D), and an–fo–pyrox–mel–liq (C). Both are quaternary reaction points. Between C and D, on the univariant line an–fo–mel–liq, lies the quaternary minimum of the tetrahedron.

The reaction role of pyroxene at the invariant point C has implications of petrologic interest, and will be considered more fully in a subsequent section.

(5) The tetrahedron *anorthite–forsterite–gehlenite–spinel.* The composition of the invariant point an–fo–sp–mel–liq lies within the tetrahedron an–geh–ak–fo, previously discussed. The two invariant points within this tetrahedron, an–geh–sp–$CaAl_{12}O_{18}$–liq (which connects to figure 4 at d) and an–sp–corundum–$CaAl_{12}O_{18}$–liq (which connects to figure 4 at j) have been discussed by DeVries and Osborn (1957) and require no further mention here.

(6) The tetrahedron *anorthite–forsterite–spinel–cordierite.* Inasmuch as the univariant line an–fo–sp–liq does not cut the face an–fo–sp (DeVries and Osborn, 1957), the quaternary invariant point an–fo–sp–cord–liq (F, fig. 4) cannot lie within this tetrahedron. The tetrahedron contains one invariant reaction point, M, mu–sp–sap–cord–liq; the univariant line mu–cord–sp–liq, which emanates from this reaction point, leaves the tetrahedron through the face anorthite–forsterite–cordierite.

(7) The tetrahedron *anorthite–forsterite–diopside–enstatite.* The four bounding planes are as follows:

(i) Anorthite–diopside–enstatite (Hytönen and Schairer, 1960) contains a piercing point, an–pyrox–fo–liq.

(ii) Anorthite–diopside–forsterite (Osborn and Tait, 1952) contains two piercing points, an–pyrox–fo–liq and an–sp–fo–liq.

(iii) Anorthite–enstatite–forsterite (Andersen, 1915) contains a piercing point, an–sp–fo–liq.

(iv) Diopside–enstatite–forsterite (Ricker and Osborn, 1954) contains a three-phase line running from the diopside–enstatite join to the diopside–forsterite join, along which forsterite, pyroxene, and liquid are in equilibrium.

The tetrahedron thus contains no invariant points, only two univariant lines—an–fo–di–liq and an–fo–sp–liq.

It must be noted here that the effect of the immiscibility gap between diopside and enstatite shown by Boyd and Schairer (1957) will be to introduce two piercing points, fo–di–ens–liq and ens–di–tr–liq, into the system CaO–MgO–SiO_2 (Osborn and Muan, 1960), and hence two extra quaternary invariant points (ens–di–an–fo–liq, X, and an–ens–di–tr–liq, Y, connected by the line an–ens–di–liq) into the system CaO–MgO–Al_2O_3–SiO_2. The compositions of X and Y lie within the tetrahedron an–ens–di–SiO_2, previously considered by Osborn and Tait (1952); as the immiscibility gap between diopside and enstatite at liquidus temperatures was unknown at the time of Osborn and Tait's work, these authors did not deduce the presence of the two invariant points. The tetrahedron an–fo–di–SiO_2 will be further considered in the section on petrologic implications.

(8) The tetrahedron *anorthite–forsterite–enstatite–cordierite*. Of the bounding planes, none is ternary:

(i) Enstatite–forsterite–cordierite (Rankin and Merwin, 1918) contains two piercing points, cord–fo–ens–liq and fo–sp–cord–liq.

(ii) Anorthite–cordierite–forsterite (fig. 6) contains one piercing point, sp–mu–cord–liq.

(iii) Anorthite–enstatite–forsterite (Andersen, 1915) contains one piercing point, an–fo–sp–liq.

(iv) Anorthite–enstatite–cordierite (fig. 6) contains four piercing points: an–fo–sp–liq, fo–sp–cord–liq, cord–fo–ens–liq, and sp–mu–cord–liq. The tetrahedron thus contains no invariant points. Four univariant lines run through the tetrahedron and plunge through the plane anorthite–enstatite–cordierite into

(9) The tetrahedron *anorthite–enstatite–cordierite–silica*. Of the planes other than an–ens–cord, just discussed,

(i) Anorthite–enstatite–silica (Andersen, 1915) contains two piercing points, an–fo–ens–liq and an–ens–tr–liq.

(ii) Anorthite–cordierite–silica (fig. 6) also contains two piercing points, an–mu–tr–liq and an–sp–mu–liq.

(iii) Cordierite–enstatite–silica (Rankin and Merwin, 1918) contains the piercing points ens–cord–tr–liq and cord–mu–tr–liq.

The tetrahedron would thus appear to contain the remarkable complement of five quaternary invariant points, four of which (an–ens–cord–fo–liq, E; an–fo–sp–cord–liq, F; an–cord–mu–tr–liq, J; an–cord–mu–sp–liq, K) are reaction points leading the eutectic an–ens–cord–tr–liq, I. This eutectic forms a silica-rich "sink"; with equilibrium crystallization the final liquids of all compositions within the volume an–fo–sp–mu–silica will lie within this tetrahedron.

Petrologic implications.—The most interesting aspect of the flow-sheet of figure 4 lies in the reaction relationship of pyroxene at the invariant point C. This may be discussed more fully in terms of the relevant tetrahedra anorthite–gehlenite–akermanite–forsterite and anorthite–diopside–akermanite–forsterite. Because of the difficulty of visualizing crystallization paths in "three-dimensional" perspective drawings, the two tetrahedra are represented in

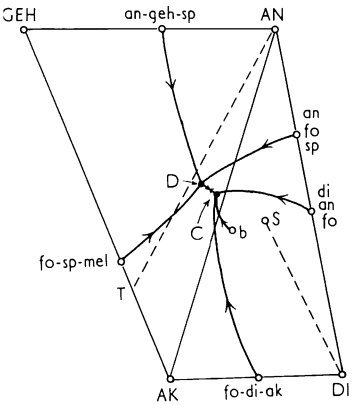

Fig. 7. Projection of univariant lines and invariant points in the tetrahedra anorthite–gehlenite–akermanite–forsterite and diopside–anorthite–akermanite–forsterite from the forsterite apices on to the bases an–geh–ak and di–an–ak. DI-S is the projection of part of the line of solid solution of "Ca Tschermakite" in diopside; S represents the pyroxene composition 30 weight percent $CaAl_2SiO_6$. T is the composition $Geh_{25}Ak_{75}$ on the melilite join. Abbreviations, and letters denoting invariant points and piercing points, as in figure 4.

figure 7 as projections from the forsterite apices onto the almost coplanar bases anorthite–gehlenite–akermanite and anorthite–akermanite–diopside. This mode of projection is unlikely to have produced serious distortion in the relative positions of the univariant lines, since in the bounding faces the compositions of the piercing points all contain less than 20 percent forsterite. Part of the line of solid solution of "Ca Tschermakite" in diopside, which runs from diopside into the tetrahedron anorthite–diopside–akermanite–forsterite at a small angle to the plane anorthite–akermanite–diopside, is shown in the projection by the line DI-S.

Although the four-phase tie lines along the univariant lines are unknown, the geometry of the tetrahedra strongly suggests that at the temperature maxima on the univariant lines an–pyrox–fo–liq, fo–pyrox–mel–liq, and an–mel–pyrox–liq (where these lines intersect, respectively, the planes anorthite–diopside–forsterite, forsterite–diopside–akermanite, and anorthite–akermanite–diopside) the composition of the pyroxene is close to pure diopside. Thus Osborn and Tait (1952) and de Wys and Foster (1958) have been able to treat an–di–fo and an–ak–di, respectively, as essentially ternary systems. As the univariant lines descend from the temperature maxima towards the invariant point C, however, the composition of the pyroxene in equilibrium with liquid will increase in aluminum content, probably reaching the maximum "Ca Tschermakite" content at point C, where the pyroxene reacts with liquid to give essentially an akermanite-rich melilite, and anorthite. The pyroxenes will thus also have a reaction relationship to liquids descending along the univariant lines, as they will continually increase in Al_2O_3 content as C is approached. The effect of the removal by fractionation of early-formed diopsidic pyroxene would thus be to enrich the liquid in alumina and lime, thus ultimately enriching the crystallization products of the final liquid in melilite.

Since the univariant lines trend generally towards the CaO apex of the tetrahedron CaO–MgO–Al_2O_3–SiO_2, the addition of lime to a liquid descending along one of the univariant lines would accentuate this behavior.

The role of pyroxene in this system shows striking parallels with the behavior of pyroxenes in the classic example of olivine diabase contaminated by limestone at Scawt Hill, Northern Ireland (Tilley and Harwood, 1931). In these rocks the first product of contamination was a pyroxenite consisting mainly of an aluminum-poor diopside, the precipitation of which presumably liberated the heat required for lime assimilation. Later-formed pyroxenes contain up to 19 percent $CaAl_2SiO_6$ and give clear evidence of reaction with liquid to form melilite. The final product of the contamination-differentiation sequence is a melilite rock virtually free of pyroxene.

The Scawt Hill differentiation process is accompanied by the desilication of the albite component of plagioclase to form nepheline, which later reacts with liquid to produce a $CaNaAlSi_2O_7$ "component" in the melilites, while the Fe/Mg ratio of the differentiates rises. The presence of H_2O and CO_2 in the gas phase must also have been of great importance in modifying differentiation trends, so that interpretation of the natural phenomena in terms of the simple system CaO–MgO–Al_2O_3–SiO_2 must be made with great caution. However, an important feature of the Scawt Hill process does appear to be that demonstrated in the synthetic system—the role of aluminous pyroxene in regulating the lime and alumina content of the melt for the ultimate production of melilite.

The reaction behavior of aluminous pyroxene appears to be of significance only in liquids that descend to the melilite minima. On figure 4 the dashed line efgh represents a high-temperature "ridge" on the divariant surfaces that separates liquids that trend towards silica from those that trend towards melilite. From the viewpoint of igneous petrology it represents, in the alkali-free system, the barrier discussed by Yoder and Tilley (1957) that separates liquids taking a saturated, or tholeiitic, trend, from liquids taking an undersaturated, or alkaline trend. It is therefore of interest to consider the position of this barrier with regard to the tetrahedron anorthite–forsterite–diopside–enstatite, in which the composition of the "simplified basalt" (representing rocks predominantly containing normative olivine, hypersthene, diopside, and anorthite) will lie.

Figure 8 is a perspective representation of the tetrahedron anorthite–forsterite–diopside–silica, showing the plane anorthite–diopside–enstatite and the approximate relative positions of univariant lines and invariant points involving anorthite. The tetrahedron anorthite–forsterite–diopside–enstatite, as previously discussed, contains two univariant lines, an–fo–sp–liq and an–di–fo–liq. The maximum, e, on the an–fo–sp–liq line (i.e. where the univariant line cuts the plane anorthite–forsterite–$di_{52}ens_{48}$, which is the extension of the plane anorthite–forsterite–spinel) lies within this tetrahedron, as may be seen from the equation

$$\underset{\text{anorthite}}{CaAl_2Si_2O_8} + 2\,\underset{\text{forsterite}}{Mg_2SiO_4} = \underset{\text{spinel}}{MgAl_2O_4} + \underset{\text{diopside}}{CaMgSi_2O_6} + 2\,\underset{\text{enstatite}}{MgSiO_3}$$

The position of the maximum f on the line an–di–fo–liq is not precisely known.

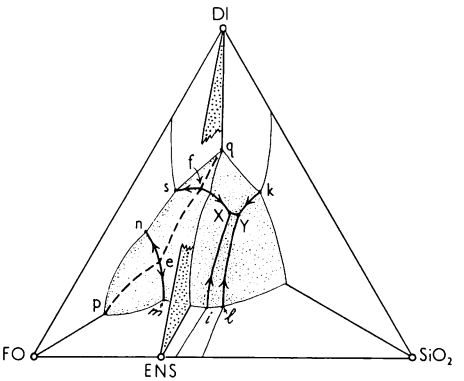

Fig. 8. The tetrahedron diopside–forsterite–anorthite–silica, showing approximate relationships of univariant lines (heavy lines) and invariant points. Intersections of the divariant surfaces with the bounding planes of the tetrahedron (cf. Osborn and Tait, 1952, fig. 7) are shown as light lines; certain divariant surfaces are shown lightly stippled. The portion of the temperature maximum efgh (fig. 4) that lies within the terahedron an–fo–di–ens is shown by the heavy dashed line pefq; nem is the univariant line an–fo–sp–liq, while sfX is the univariant line an–di–fo–liq. Other letters denoting lines and points as in figure 4. For the sake of clarity, the univariant lines ens–di–fo–liq and ens–di–tr–liq, which descend from the face di–fo–SiO_2 (Osborn and Muan, 1960) to the invariant points X and Y respectively, have been omitted, and a portion of the plane diopside–enstatite–anorthite (heavily stippled) has been cut away. Anorthite (not marked) forms the rear apex of the tetrahedron.

The temperature of the point where the univariant line pierces the plane di–an–fo is given by Osborn and Tait (1952) as 1270°. and the piercing point on the plane di–an–ens is given by Hytönen and Schairer (1960) as 1262°. As these temperatures were determined at separate laboratories, the small difference of 10° between them must be considered within the limits of experimental error. However, the maximum f presumably lies somewhere between the planes di–an–fo and di–an–ens. The temperature "ridge" efgh on the divariant surface thus passes through the tetrahedron an–fo–di–ens, entering along the join an–fo at 1444°, passing through e (1320°) and f (between 1270° and 1290°?), and leaving the tetrahedron through the join an–di (1274°) (Osborn and Tait. 1952). In the system CaO–MgO–Al_2O_3–SiO_2, therefore. liquids corresponding to the "simplified basalt" could proceed on differentiation trends leading to either saturated (silica-bearing) or undersaturated (melilite-bearing) compositions, depending on the relative proportions of "normative" forsterite, diopside, enstatite. and anorthite in the original liquid. The Scawt Hill diabase just mentioned (normative constituents Ol. 11.9; Di. 20.0; An, 33.4; Hy, 7.1, the remaining 27.6 percent being predominantly albite) has clearly taken the undersaturated trend, the assimilation of lime accentuating, but not necessarily initiating, the process. The temperature differences in the vicinity of the maximum f are, however, so small that additional components could well alter drastically the phase relations here presented. In particular, the change in the position of the maximum pefq (fig. 8) by change in water pressure might provide a mechanism whereby a particular basalt composition could take both the saturated and the undersaturated trend

and thus fulfill the requirements of the long-sought parental basalt (Yoder and Tilley, 1957).

On the silica-rich side of the temperature ridge efgh, the large number of reaction points graphically illustrates the principles of silica enrichment by the fractional crystallization of forsterite and spinel originally developed by Bowen. From the petrological viewpoint, the trend fXY and the series of more aluminous reaction points E, F, J, K, L, M, leading to the eutectic I (fig. 4) are of greatest interest. The line fXY trends generally towards the Si–Al join of the tetrahedron CaO–MgO–Al_2O_3–SiO_2, so that addition of Si or Al to liquids along it will accentuate their tendency to reach Y. This of course is merely a restatement of the old deduction (Bowen, 1928) that contamination of basaltic or gabbroic liquid by silica and alumina should convert diopside and olivine to anorthite and enstatite. Thus in the many natural examples (Lacroix, 1899; Read, 1935), contamination by argillaceous material of olivine gabbro (represented by the univariant line fX, di–an–fo–liq) has produced, firstly, norites (XY, an–ens–di–liq) and then quartz–norites (represented by Y, an–ens–di–tr–liq, or 1Y, an–ens–tr–liq).

Contaminated gabbros of this type commonly show narrow heterogeneous zones of noritic rock containing cordierite, anorthite, quartz, and enstatite (with almandine garnet, orthoclase, and biotite), which abut the country rock contacts and contain large quantities of spinel- or corundum-rich xenoliths (Read, 1935). Such cordierite–norites, which correspond to the eutectic I, an–ens–cord–tr–liq), are normally interpreted as the end product of the reaction between gabbro and country rock, the excess alumina being stored in corundum and spinel concentrated within the original xenoliths. In the system CaO–MgO–Al_2O_3–SiO_2, however, it does not appear possible to proceed from a quartz–norite (Y) to a cordierite–norite (I), for eutectic Y is separated from the more aluminous reaction points E, I, etc., by the high-temperature "ridge" il on the divariant surfaces an–ens–liq and an–tr–liq. Once a liquid has reached a temperature lower than that of l, it cannot proceed farther than Y by assimilation; one would expect to find relicts of aluminous and siliceous contaminating material remaining as xenoliths within a norite free of cordierite. Of course, in the more complex natural systems, the high-temperature "ridge" corresponding to il may become ineffective—for example, in the system CaO–MgO–Al_2O_3–SiO_2 at 10,000 bars H_2O pressure (Yoder and Chinner, 1960), the join anorthite–forsterite–enstatite (on which the maximum i depends) is replaced by diopside–enstatite–spinel. However, the existence in the dry system of the high-temperature ridge il does suggest the possibility that cordierite- and garnet-bearing norites at igneous contacts may not be so much the end products of the gabbro–norite contamination sequence as the result of the formation of a liquid corresponding in composition to the low-temperature eutectic I (fig. 4) by partial fusion of the country rock xenoliths. Assuming the availability of sufficient heat, many argillaceous rocks could give relatively large quantities of liquid corresponding to mixtures of cordierite, enstatite, quartz, and feldspar, leaving only small amounts of "excess" components concentrated in residual xenoliths. The garnet–cordierite rocks described by Read (1935, p. 610) from the Haddo House complex of Aberdeenshire as forming

"irregular patches" in country rock hornfels and containing "innumerable xenoliths of sedimentary material" could well be of such a fusion origin.

Certainly, at the contacts of many high-temperature basaltic and andesitic intrusions the production of low melting-point liquids corresponding in composition to the eutectic I (fig. 4) by the partial melting of argillaceous and arkosic country rock is very well known (Wyllie, 1959). A particularly fine example occurs at Strachur, Argyll, where, at the contact of an olivine diabase plug, a hypersthene–quartz–cordierite–feldspar assemblage produced by the fractional melting of chlorite–muscovite–quartz country rock is found veining its parent schist (S. O. Agrell, personal communication). It is apparent, however, that one must be wary of interpreting compositional changes found at small-scale igneous contact zones too rigidly in terms of crystal–liquid phase relationships. At near-solidus temperatures in plutonic intrusions diffusive effects appear to play an important role in the development of "mixed" rocks: obvious examples are provided by the development of alkaline facies in granitic rocks at contacts with limestone (Tilley, 1949). In such cases the restrictions imposed by crystal-liquid equilibrium relationships upon the possible ways in which the composition of a liquid may change are no longer applicable.

ACKNOWLEDGMENTS

We are grateful to Hatten S. Yoder Jr. and to C. E. Tilley for reading and discussing the manuscript, and to P. L. Roedder for discussions on his own analysis of phase relations in the system CaO–MgO–Al_2O_3–SiO_2.

REFERENCES

Andersen, O., 1915, The system anorthite–forsterite–silica: Am. Jour. Sci., 4th ser., v. 39, p. 407-454.

Bowen, N. L., 1928, The evolution of the igneous rocks: Princeton, Princeton University Press, x, 334 p.

Boyd, F. R., and Schairer, J. F., 1957, The join $MgSiO_3$–$CaMgSi_2O_6$: Carnegie Inst. Washington Year Book 56, p. 223-225.

Chinner, G. A., Boyd, F. R., and England, J. L., 1960, Physical properties of garnet solid-solutions: Carnegie Inst. Washington Year Book 59, p. 76-78.

Chinner, G. A., and Schairer, J. F., 1959, The join grossularite–pyrope at atmospheric pressure: Carnegie Inst. Washington Year Book 58, p. 107-109.

DeVries, R. C., and Osborn, E. F., 1957, Phase equilibria in high-alumina part of the system CaO–MgO–Al_2O_3–SiO_2: Am. Ceram. Soc. Jour., v. 40, p. 6-15.

Ervin, G., and Osborn, E. F., 1949, X-ray data on synthetic melilites: Am. Mineralogist, v. 34, p. 717-722.

Hytönen, K., and Schairer, J. F., 1960, The system enstatite–anorthite–diopside: Carnegie Inst. Washington Year Book 59, p. 71-72.

Keith, M. L., and Schairer, J. F., 1952, The stability field of sapphirine in the system MgO–Al_2O_3–SiO_2: Jour. Geology, v. 60, p. 181-186.

Lacroix, A., 1899, Le gabbro du Pallet et ses modifications: Service carte géol. France Bull. 10, p. 341-392.

Osborn, E. F., 1942, The system $CaSiO_3$–diopside–anorthite: Am. Jour. Sci., v. 240, p. 751-758.

Osborn, E. F., DeVries, R. C., Gee, K. G., and Kraner, H. M., 1954, Optimum composition of blast-furnace slag as deduced from liquidus data for the quaternary system CaO–MgO–Al_2O_3–SiO_2: Jour. Metals, Jan. 1954, p. 3-15.

Osborn, E. F., and Muan, Arnulf, 1960, The system CaO–MgO–SiO_2: Columbus, Ohio, American Ceramic Society, Plate 2.

Osborn, E. F., and Schairer, J. F., 1941, The ternary system pseudowollastonite–akermanite–gehlenite: Am. Jour. Sci., v. 239, p. 715-763.

Osborn, E. F., and Tait, D. B., 1952, The system diopside–forsterite–anorthite: Am. Jour. Sci., Bowen vol., p. 413-433.

Prince, A. T., 1954, Liquidus relationships on 10% MgO plane of the system lime–magnesia–alumina–silica: Am. Ceram. Soc. Jour., v. 37, p. 402-408.

Rankin, G. A., and Merwin, H. E., 1918, The ternary system $MgO–Al_2O_3–SiO_2$: Am. Jour. Sci., 4th ser., v. 45, p. 301-325.

Rankin, G. A., and Wright, F. E., 1915, The ternary system $CaO–Al_2O_3–SiO_2$: Am. Jour. Sci., 4th ser., v. 39, p. 1-79.

Read, H. H., 1935, The gabbros and associated xenolithic complexes of the Haddo House district, Aberdeenshire: Geol. Soc. London Quart. Jour., v. 91, p. 591-638.

Ricker, R. W., and Osborn, E. F., 1954, Additional phase data for the system $CaO–MgO–SiO_2$: Am. Ceram. Soc. Jour., v. 37, p. 133-139.

Roy, D. M., and Roy, Rustum, 1955, Synthesis and stability of minerals in the system $MgO–Al_2O_3–SiO_2–H_2O$: Am. Mineralogist, v. 40, p. 147-178.

Sakata, Y., 1957, Unit-cell dimensions of syntheetic aluminian diopsides: Japanese Jour. Geology and Geography, v. 28, p. 161-168.

Schairer, J. F., 1942, The system $CaO–FeO–Al_2O_3–SiO_2$: I, Results of quenching experiments on five joins: Am. Ceram. Soc. Jour., v. 25, p. 241-274.

———— 1959, Phase equilibria with particular reference to silicate systems, *in* Bockris, J. O., MacKenzie, J. D., and White, J. L., eds., Physiochemical measurements at high temperatures: London, Butterworths Scientific Publications, p. 117-134.

Segnit, E. R., 1953, Some data on synthetic aluminous and other pyroxenes: Mineralog. Mag., v. 30, p. 218-226.

———— 1956, The section $CaSiO_3–MgSiO_3–Al_2O_3$: Mineralog. Mag., v. 31, p. 255-264.

Tilley, C. E., 1923, Paragenesis of the minerals of the three component system $MgO–Al_2O_3–SiO_2$ in thermal metamorphism: Geol. Mag., v. 60, p. 101-107.

———— 1949, An alkali facies of granite at granite-dolomite contacts in Skye: Geol. Mag., v. 86, p. 81-93.

———— 1952, Some trends of basaltic magma in limestone syntexis: Am. Jour. Sci., Bowen vol., p. 529-545.

Tilley, C. E., and Harwood, H. F., 1931, The dolerite-chalk contact of Scawt Hill, Co. Antrim: Mineralog. Mag., v. 22, p. 439-468.

Wyllie, P. J., 1959, Microscopic cordierite in fused Torridonian arkose: Am. Mineralogist, v. 44, p. 1039-1046.

Wys, E. C. de, and Foster, W. R., 1958, The system diopside–anorthite–akermanite: Mineralog. Mag., v. 31, p. 736-743.

Yoder, H. S., 1950, Stability relations of grossularite: Jour. Geology, v. 58, p. 221-253.

———— 1952, The $MgO–Al_2O_3–SiO_2–H_2O$ system and the related metamorphic facies: Am. Jour. Sci., Bowen vol., p. 569-627.

Yoder, H. S., and Chinner, G. A., 1960, Grossularite–pyrope–water system at 10,000 bars: Carnegie Inst. Washington Year Book 59, p. 78-81.

Yoder, H. S., and Tilley, C. E., 1957, Basalt magmas: Carnegie Inst. Washington Year Book 56, p. 156-161.

Zvetkov, A. I., 1945, Synthesis of alumina pyroxenes and dependence of their optics on composition: Soc. Min. Russe Bull., v. 74, p. 215-222 [in Russian].